EARTHQUAKE ENGINEERING AND STRUCTURAL DYNAMICS
Earthquake Engng Struct. Dyn. 2005; **34**:965–983
Published online 31 January 2005 in Wiley InterScience (www.interscience.wiley.com). DOI: 10.1002/eqe.464

Semi-active control of sliding isolated bridges using MR dampers: an experimental and numerical study

Sanjay S. Sahasrabudhe[1,2] and Satish Nagarajaiah[2,*,†]

[1]*Structural Engineering Department, J. Ray McDermott Eng. LLC, Houston TX 77079, U.S.A.*
[2]*Departments of Civil and Environmental Engineering, and Mechanical Engineering and Materials Science, Rice University, Houston, TX 77005, U.S.A.*

SUMMARY

Sliding base-isolation systems used in bridges reduce pier drifts, but at the expense of increased bearing displacements under near-source pulse-type earthquakes. It is common practice to incorporate supplemental passive non-linear dampers into the isolation system to counter increased bearing displacements. Non-linear passive dampers can certainly reduce bearing displacements, but only with increased isolation level forces and pier drifts. The semi-active controllable non-linear dampers, which can vary damping in real time, can reduce bearing displacements without further increase in forces and pier drifts; and hence deserve investigation. In this study performance of such a 'smart' sliding isolation system, used in a 1:20 scaled bridge model, employing semi-active controllable magneto-rheological (MR) dampers is investigated, analytically and experimentally, under several near-fault earthquakes. A non-linear analytical model, which incorporates the non-linearities of sliding bearings and the MR damper, is developed. A Lyapunov control algorithm for control of the MR damper is developed and implemented in shake table tests. Analytical and shake table test results are compared. It is shown that the smart MR damper reduces bearing displacements further than the passive low- and high-damping cases, while maintaining isolation level forces less than the passive high-damping case. Copyright © 2005 John Wiley & Sons, Ltd.

KEY WORDS: bridges; sliding isolation systems; controllable MR dampers; semi-active control; near-fault earthquakes; seismic response

INTRODUCTION

Base-isolation systems provide an effective means of protecting bridges and buildings against near-field earthquakes [1, 2]. In bridges, base-isolation systems reduce pier drifts and forces,

*Correspondence to: Satish Nagarajaiah, Departments of Civil and Environmental Engineering, and Mechanical Engineering and Materials Science, Rice University, Houston, TX 77005, U.S.A.
†E-mail: nagaraja@rice.edu

Contract/grant sponsor: National Science Foundation; contract/grant number: NSF-CAREER Grant CMS–9996290

Received 18 June 2004
Revised 15 November 2004
Accepted 15 November 2004

but at the expense of increased isolation level displacements. Under far-field earthquakes base-isolation systems alone are adequate. However, under near-field, high velocity pulse-type earthquakes bearings can undergo excessive displacements and fail [3]. Shen *et al.* [4], in their recent study of the elastomeric base-isolated Bai-Ho bridge in Taiwan, point out the susceptibility of base-isolated bridges under near-source earthquakes, and the need for passive/adaptive base-isolation strategies. To counter increased bearing displacements, it is common practice to include supplemental non-linear passive dampers into the isolation system [5, 6]. Providing such supplemental passive dampers can certainly reduce bearing displacements, but only with increased pier drifts and isolation level forces. Semi-active controllable non-linear dampers—which can vary damping appropriately in real time—can reduce bearing displacements and forces further than the passive dampers; and hence deserve investigation. Such base-isolation systems using passive and/or semi-active controllable devices are also known as 'smart' or 'hybrid' base-isolation systems.

Several researchers have investigated the effectiveness of semi-active devices [7]. Base-isolated bridges with elastomeric bearings and controllable fluid dampers were first studied by Kawashima *et al.* [8] and Yang *et al.* [9]. The shaking table tests reported by Kawashima *et al.* [8] show the effectiveness of variable dampers for seismic response reduction. Symans *et al.* [10] have investigated the effectiveness of controllable fluid dampers in bridges with elastomeric isolation systems, controlled using a fuzzy logic algorithm, and have shown their effectiveness in reducing the seismic response. The effectiveness of semi-active MR fluid dampers [11, 12], in reducing the seismic response of elastomeric base-isolated cable-stayed bridges has been analytically studied by Jung *et al.* [13, 14] and shown to be effective. Agrawal *et al.* [15] analytically studied applications of semi-active stiffness dampers and semi-active friction dampers in cable-stayed bridges and showed their effectiveness. Applications of semi-active electro-rheological dampers in elastomeric base-isolated structures have been studied by Makris [3] and Gavin [16], and shown to be effective in reducing seismic response. The application of hydraulic actuators in sliding isolated bridges has also been investigated by Nagarajaiah *et al.* [17]. Their experimental study showed that the active devices, controlled using an absolute acceleration feedback, are indeed very effective in near-source earthquakes. However, the large power requirement of actively controlled systems—which may not be available in an earthquake event—is a limiting factor. The effectiveness of semi-active magneto-rheological (MR) dampers, with low power requirements [11, 12], in reducing the seismic response of sliding base-isolated bridges under a variety of near-source earthquakes has not been investigated analytically or experimentally; and so deserves careful investigation.

In this paper an analytical and experimental study is presented of a 1:20 scale steel bridge model consisting of Teflon®–stainless steel sliding bearings and a magneto-rheological (MR) damper. A new analytical model of the bridge, which incorporates non-linearities of sliding bearings and the MR damper, is developed. Responses under a variety of near-source earthquakes are computed using the analytical model and compared with the shaking table test results [18]. A Lyapunov-based control algorithm for control of the MR damper and bridge model is developed and implemented in shaking table tests. Responses of the passive low- and high-damping cases are compared with the semi-active case. It is shown that the MR damper in semi-active controlled mode reduces isolation level displacements further than the passive low- and high-damping cases while maintaining isolation level forces near that of the passive low-damping case.

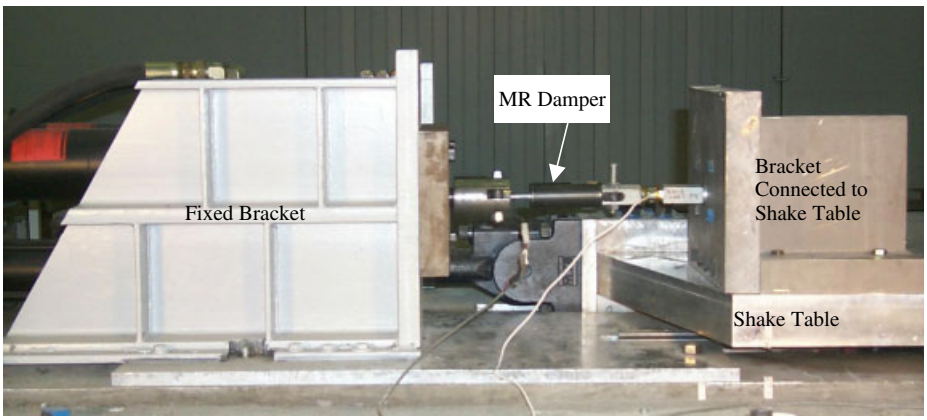

Figure 1. Test set-up for the MR damper.

MAGNETO-RHEOLOGICAL (MR) DAMPER

The MR damper (Figure 1), obtained from Lord Corporation, North Carolina, consists of MR fluid in the main cylinder (Figure 2(a)). The MR fluid consists of micron-sized iron particles suspended in silicon fluid [11]. The piston of the damper contains an annular orifice which is surrounded by a magnetic coil. An accumulator is provided at the end of the damper to prevent cavitations in the fluid. The damper is 15.2 cm long in the compressed position and the main cylinder is 4.2 cm in diameter. The damper has a stroke of 5.7 cm. The voltage supplied to the damper varies from 0 to 4 V. When the damper is stroked fluid passes through the annular orifice which is surrounded by a coil. With the application of voltage, the magnetic field in the coil changes, causing the iron particles suspended in the MR fluid to form chains. The fluid changes from viscous fluid to semi-solid, thus increasing force in the MR damper. Low power requirements of the damper augmented with short response time ($\sim$25 ms) makes it a suitable device for seismic applications [12]. In order to study the force–displacement behavior of the damper a test set-up, shown in Figure 1, has been designed and built. The test set-up has been designed to apply a displacement to the piston of the damper, and to measure forces generated by the damper. The set-up consists of a fixed bracket and a bracket connected to the shake table (Figure 1). The MR damper is connected between the two brackets. A load cell (capacity 4.45 kN) is incorporated into the assembly to measure the force generated by the damper. The displacement is imposed by a servo-hydraulic actuator and measured using a Linear Variable Displacement Transducer (LVDT). Figure 2(b) shows the experimental results under harmonic excitation of 2.5 Hz, with voltage varying from 0 to 4 V. The force–displacement responses (Figure 2(b)) demonstrate the non-linear behavior of the damper. The loops are stable and repeatable over a large number of cycles. The force in the MR damper increases with voltage, from around 220 N at 0 V to around 1350 N at 4 V.

1:20 SCALE BRIDGE MODEL WITH SLIDING BEARINGS AND MR DAMPER

Based on the laws of artificial mass simulation [19] shown in Table I, a single span 1:20 scaled bridge model has been designed and fabricated [18]. The bridge model, shown in

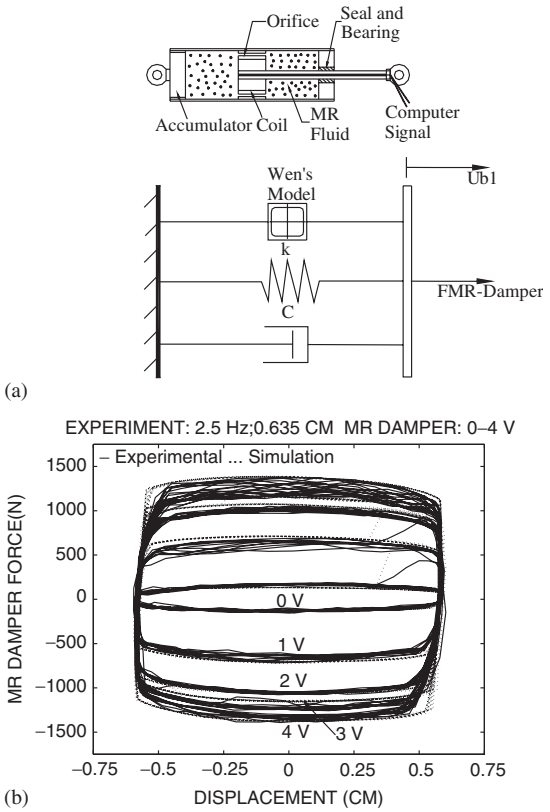

Figure 2. (a) Schematic and analytical model of MR damper; and (b) force–displacement response.

Table I. Scaling factors.

Parameter	Scaling factors	1:20 Model
Length	l_r	1/20
Time	$\sqrt{l_r}$	$1/\sqrt{20}$
Displacement	l_r	1/20
Velocity	$\sqrt{l_r}$	$1/\sqrt{20}$
Acceleration	1	1
Force	l_r^2	1/400

Figures 3 and 4 has a clear span of 1.83 m, width 0.89 m and height 0.96 m. The weight of the deck is 12.48 kN and the piers weigh 0.53 kN each. At model scale, the bridge is designed to have a natural period of 0.5 s in the isolated case and 0.1 s in the non-isolated case, i.e. 2.25 s and 0.45 s, respectively, at prototype scale. The bridge model has four sliding

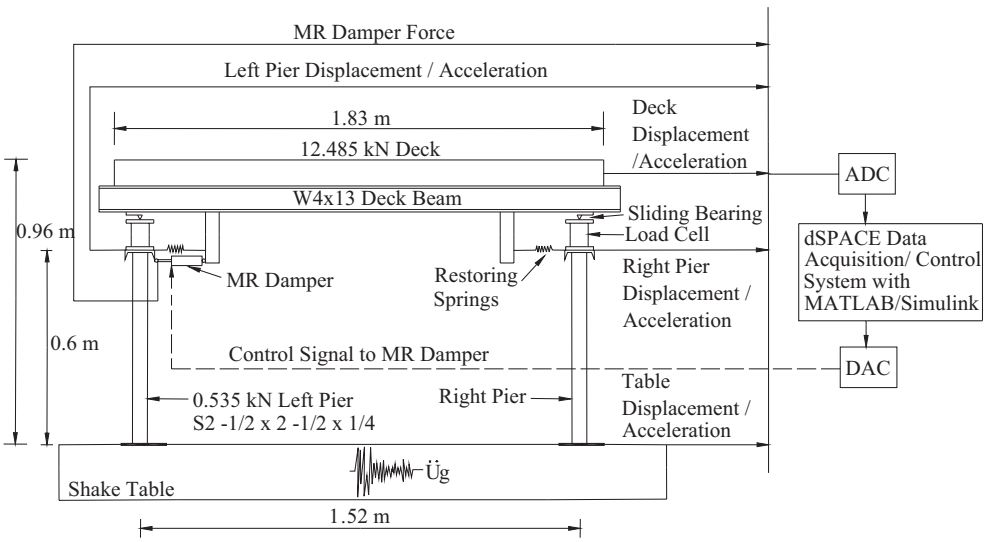

Figure 3. 1 : 20 Scale sliding isolated bridge model with MR damper and block diagram of data acquisition and control system.

bearings, consisting of Teflon®–stainless steel interfaces (Figure 4). The sliding bearings decouple the deck from the piers. The sliding bearings are supported by tri-axial load cells, which measure forces transmitted from the deck to the piers (Figure 4). The measured friction force in sliding bearings normalized with respect to the deck weight as a function of relative deck–left pier displacement response under different sinusoidal excitation frequencies is shown in Figure 5(a). The sliding bearings have a dynamic coefficient of friction of 6% at low velocity and 13% at high velocities, as shown in Figure 5(b). Four restoring springs, each having stiffness of 723 N/cm, are connected between the deck and the piers as shown in Figure 4(b). A smart MR damper is also connected between the deck and the left pier as shown in Figure 4(b). A load cell of capacity 4.45 kN is used to measure forces in the MR damper.

The bridge model was instrumented with LVDTs and accelerometers at both the piers and the deck to measure displacement and acceleration response as shown in Figure 3. A dSPACE system with MATLAB/Simulink was used to perform data acquisition and control. The block diagram of experimental data acquisition and control system is shown in Figure 3.

ANALYTICAL AND EXPERIMENTAL PROGRAM

In order to evaluate the effectiveness of the MR damper an analytical and experimental study was carefully planned. Shake table tests were performed under the isolated case with: (1) passive low damping (damping ratio ~4%)—MR damper 'off' with constant zero volts; (2)

(a)

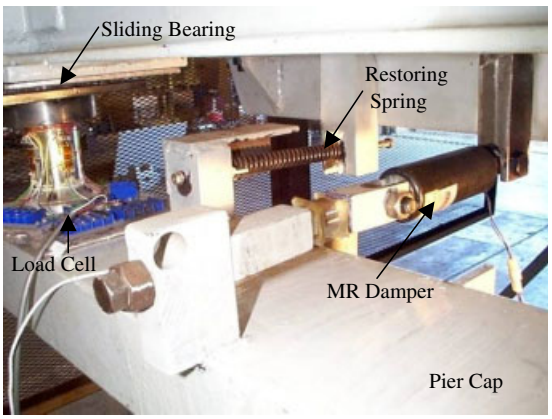

(b)

Figure 4. (a) Sliding isolated bridge model on the shake table (reference frame shown on right); and (b) close-up view of MR damper and restoring springs connected between deck and left pier.

passive high damping (damping ratio ∼35%)—MR damper 'on' with constant four volts; and (3) controlled cases in which the voltage is switched based on the developed control algorithm. Shake table tests are performed with the following scaled earthquakes.

(i) El Centro S00E earthquake (18 May 1940), peak acceleration: 0.87g
(ii) Northridge Newhall earthquake, Channel 1-90 Deg. (17 Jan. 1994), peak acceleration: 1.75g
(iii) Northridge Sylmar earthquake, Channel 1-90 Deg. (17 Jan. 1994), peak acceleration: 1.18g

The El Centro earthquake exhibits characteristics of far-field motions although it was recorded near-fault. Additionally fault normal components Newhall 360 and Sylmar 360 are also studied, results of which are presented by Sahasrabudhe [18]. As per Table I, the earthquake signals were compressed by a time scale factor of $1/\sqrt{20}$.

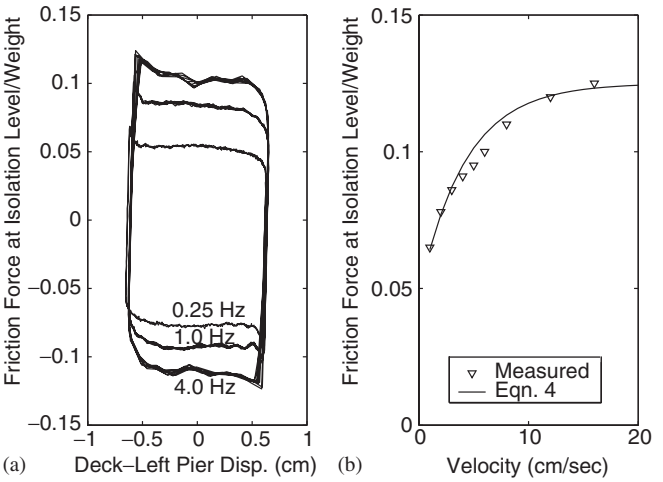

Figure 5. (a) Measured friction force/weight vs. relative displacement; and (b) variation of friction force/weight vs. velocity.

ANALYTICAL MODEL OF THE SLIDING ISOLATED BRIDGE

An analytical model of the bridge, which takes into account the non-linearities of frictional sliding bearings and the MR damper, has been developed [18]. The mass of the deck is $12.72\,\mathrm{Ns}^2/\mathrm{cm}$. The mass of each pier is $0.54\,\mathrm{Ns}^2/\mathrm{cm}$. The equations of motion are:

$$m_{\mathrm{d}}\ddot{U}_{\mathrm{d}} + F_{\mathrm{b1}} + F_{\mathrm{b2}} + F_{\mathrm{spr}} + F_{\mathrm{MR}} = -m_{\mathrm{d}}\ddot{U}_g \tag{1}$$

$$m_{\mathrm{p1}}\ddot{U}_{\mathrm{p1}} + F_{\mathrm{p1}} - F_{\mathrm{b1}} - F_{\mathrm{spr}}/2 - F_{\mathrm{MR}} = -m_{\mathrm{p1}}\ddot{U}_g \tag{2}$$

$$m_{\mathrm{p2}}\ddot{U}_{\mathrm{p2}} + F_{\mathrm{p2}} - F_{\mathrm{b2}} - F_{\mathrm{spr}}/2 = -m_{\mathrm{p2}}\ddot{U}_g \tag{3}$$

where $U_{\mathrm{d}}, U_{\mathrm{p1}}, U_{\mathrm{p2}}$ are the deck, left pier and right pier displacements relative to the shake table, respectively; $\ddot{U}_g$ is the ground acceleration; $\ddot{U}_{\mathrm{d}}, \ddot{U}_{\mathrm{p1}}, \ddot{U}_{\mathrm{p2}}$ are the deck, left pier and right pier accelerations, respectively; $m_{\mathrm{d}}, m_{\mathrm{p1}}, m_{\mathrm{p2}}$ are the deck, left pier and right pier masses, respectively; F_{b1} and F_{b2} are the frictional forces in the sliding bearings at the left and right piers, respectively; F_{MR} is the force generated in the MR damper; $F_{\mathrm{spr}} = k_{\mathrm{spr}} U_{\mathrm{b}i}$ is the total force in the restoring springs, where k_{spr} is the stiffness of restoring springs (each 723 N/cm stiffness); $U_{\mathrm{b}i} = U_{\mathrm{d}} - U_{\mathrm{p}i}$ is the relative displacement between the deck and pier i; and $F_{\mathrm{p1}}, F_{\mathrm{p2}}$ are resisting forces in the piers. The piers are assumed as lumped mass systems, since most of the mass of the piers is concentrated at the top.

The force in sliding bearings is $f_{\mathrm{s}} = F_{\mathrm{b1}} + F_{\mathrm{b2}}$, where $F_{\mathrm{b}i} = \mu_i w_i z_i$, and μ_i is the coefficient of friction at pier i, w_i is the normal load on the sliding bearing at pier i, and z_i is the Wen's [20] hysteresis variable for friction, given by Equation (5). The coefficient of dynamic sliding friction [21, 22] is given by:

$$\mu_i = f_{\max\_i} - (f_{\max\_i} - f_{\min\_i})\mathrm{e}^{-(a_i * \mathrm{abs}(\dot{U}_{\mathrm{b}i}))} \tag{4}$$

where $f_{\max\_i} = 0.13$, $f_{\min\_i} = 0.06$, and $a_i = 0.2362\,\mathrm{s/cm}$.

The hysteresis variable z for friction is obtained by solving Equation (5) with $Y_i = 0.127\,\text{cm}$ —small yield displacement of Teflon® bearing before sliding, $\gamma = 0.9$ and $\beta = 0.1$.

$$Y_i \dot{z}_i + \gamma |\dot{U}_{bi}| z_i |z_i| + \beta \dot{U}_{bi} z_i^2 - \dot{U}_{bi} = 0 \tag{5}$$

From the analytical model of the MR damper shown in Figure 2(a), the force in the damper is:

$$f_c = F_{MR} = (\alpha^* z)^* f(v) + C^* \dot{U}_{b1} + k^* U_{b1} \tag{6}$$

where $k = 8.24\,\text{N/cm}$, $\alpha = (66.9 + 258.6^* v)\,\text{N}$, $C = 7.2 + 5.87 * v\,\text{Ns/cm}$, and the non-dimensional parameter $f(v) = \beta_3^* v^3 - \beta_2^* v^2 + \beta_1^* v + \beta_0$ (where $\beta_0 = 0.8133$, $\beta_1 = 1.3706$, $\beta_2 = 0.6679$, and $\beta_3 = 0.0808$, with appropriate dimensions). The voltage supplied to the MR damper is v. The best fit parameters were obtained from the harmonic test results of the MR damper. The hysteresis variable z for the MR damper is obtained by solving Equation (5) with $Y_i = 0.165\,\text{cm}$.

The corresponding state, measured output, and regulated output equations are as follows:

$$\dot{\boldsymbol{x}}(t) = \boldsymbol{A}\boldsymbol{x}(t) + \boldsymbol{B} f_c(t) + \boldsymbol{B} f_s(t) + \boldsymbol{E}\ddot{U}_g(t) \tag{7}$$

$$\boldsymbol{y}(t) = \boldsymbol{C}_m \boldsymbol{x}(t) + \boldsymbol{D}_m f_c(t) + \boldsymbol{D}_m f_s(t) + \boldsymbol{E}_m \ddot{U}_g(t) \tag{8}$$

$$\boldsymbol{z}(t) = \boldsymbol{C}_z \boldsymbol{x}(t) + \boldsymbol{D}_z f_c(t) + \boldsymbol{D}_z f_s(t) + \boldsymbol{E}_z \ddot{U}_g(t) \tag{9}$$

where $\boldsymbol{A}, \boldsymbol{B}, \boldsymbol{C}_m, \boldsymbol{C}_z, \boldsymbol{D}_m, \boldsymbol{D}_z, \boldsymbol{E}, \boldsymbol{E}_m, \boldsymbol{E}_z, \dot{\boldsymbol{x}}(t), \boldsymbol{x}(t), \boldsymbol{y}(t), \boldsymbol{z}(t)$ are appropriately defined system matrices or vectors. The measured outputs are absolute accelerations at the deck and both the piers. The measured accelerations can be passed through a second-order filter [23] to obtain absolute or total velocities and displacements.

The non-linear equations of motion are solved using an iterative pseudo-force method [21, 22]. The equations of motion (Equations (1)–(3)) are solved using the unconditionally stable Newmark's constant-average acceleration method. The differential equations governing the behavior of the non-linear sliding isolation elements (Equation (4)) and the MR damper (Equation (6)) are solved using the unconditionally stable semi-implicit Runge–Kutta method. An iterative procedure consisting of corrective pseudo-forces is employed within each time step until equilibrium is achieved.

CONTROL ALGORITHM

A Lyapunov-based control algorithm is presented here. Assuming the piers to be rigid, the control algorithm is developed based on a representative single degree-of-freedom model. The equations of motion are

$$m\ddot{u}_a + k(u_a - u_g) + f_s + f_c = 0 \tag{10}$$

where m is total mass, k is the restoring spring stiffness, u_g is shake table displacement, u_r is the relative displacement of mass with respect to shake table, and u_a is the absolute or total displacement of mass. Substituting $f_c = c_v \dot{\boldsymbol{u}}_r$ with $u_r = u_a - u_g$, and rewriting the equations of motions:

$$\ddot{u}_a = -\frac{k}{m}(u_a - u_g) - \frac{f_s}{m} - \frac{f_c}{m} \tag{11}$$

which can be formulated in state space as

$$\begin{Bmatrix} \dot{u}_{1a} \\ \dot{u}_{2a} \end{Bmatrix} = \begin{Bmatrix} \dot{u}_a \\ \ddot{u}_a \end{Bmatrix} = \begin{bmatrix} 0 & 1 \\ -k/m & 0 \end{bmatrix} \begin{Bmatrix} u_a \\ \dot{u}_a \end{Bmatrix} - \begin{Bmatrix} 0 \\ 1/m \end{Bmatrix} f_s - \begin{Bmatrix} 0 \\ 1/m \end{Bmatrix} f_c + \begin{Bmatrix} 0 \\ 1/m \end{Bmatrix} k u_g \tag{12}$$

Thus Equation (12) can be written as:

$$\dot{U}_a = AU_a - Bf_s - Bf_c + Bku_g \tag{13}$$

where $A = \begin{bmatrix} 0 & 1 \\ -k/m & 0 \end{bmatrix}$, and $B = \begin{Bmatrix} 0 \\ 1/m \end{Bmatrix}$.

The Lyapunov function V is defined as

$$V = \tfrac{1}{2}\,\sigma^{\mathrm{T}}(U_a)\sigma(U_a) \tag{14}$$

where

$$\sigma(U_a) = P^{\mathrm{T}}U_a = [P_1 \;\; P_2] \begin{Bmatrix} u_a \\ \dot{u}_a \end{Bmatrix} \tag{15}$$

Choosing $P_1 = \sqrt{k}$ and $P_2 = \sqrt{m}$ yields $V = \frac{1}{2}\,ku_a^2 + \sqrt{k}\,\sqrt{m}u_a\dot{u}_a + \frac{1}{2}\,m\dot{u}_a^2$, where the first term represents the total strain energy in the spring, the second term represents the total dissipated energy, and the third term represents the total kinetic energy.

$$\dot{V} = \sigma^{\mathrm{T}}(U_a)\dot{\sigma}(U_a) = U_a^{\mathrm{T}}PP^{\mathrm{T}}\dot{U}_a \tag{16}$$

Simplifying Equation (16) we get:

$$\dot{V} = \sigma(U_a)P^{\mathrm{T}}B\dot{u}_r\left(-c_v + \frac{1}{\dot{u}_r}\left(\frac{m}{P_2}P_1\dot{u}_a - ku_r - f_s\right)\right) \tag{17}$$

Since only the first term c_v can be varied for $\dot{V}$ to be negative or minimum

$$c_v = \begin{cases} C_{\max} & \sigma^{\mathrm{T}}(U_a)P^{\mathrm{T}}B\dot{u}_r > 0 \\ 0 \text{ or } C_{\min} & \sigma^{\mathrm{T}}(U_a)P^{\mathrm{T}}B\dot{u}_r < 0 \end{cases} \tag{18}$$

which can be written as

$$c_v = \begin{cases} C_{\max} & \dfrac{P_2}{m}(P_1u_a + P_2\dot{u}_a)\dot{u}_r > 0 \\ 0 \text{ or } C_{\min} & \dfrac{P_2}{m}(P_1u_a + P_2\dot{u}_a)\dot{u}_r < 0 \end{cases} \tag{19}$$

Substituting $P_1 = \sqrt{k}$ and $P_2 = \sqrt{m}$ leads to

$$c_v = \begin{cases} C_{\max} & (\omega_n u_a + \dot{u}_a)\dot{u}_r > 0 \\ 0 \text{ or } C_{\min} & (\omega_n u_a + \dot{u}_a)\dot{u}_r < 0 \end{cases} \tag{20}$$

where c_v = variable damping coefficient of the MR damper; $C_{\min}$ = minimum damping coefficient for 1 V; and $C_{\max}$ = maximum damping coefficient for 4 V. Simulations lead to the

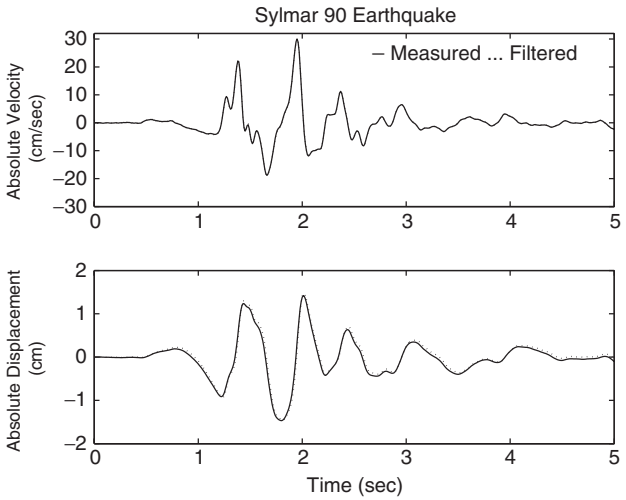

Figure 6. Comparison of measured and filtered absolute or total velocity and displacement under Sylmar 90.

introduction of a non-dimensional constant $\alpha = 14.3$ ($\omega_n = 7$ rad/s) for optimal response reduction, i.e. $(\alpha\omega_n u_a + \dot{u}_a)\dot{u}_r$ being the condition to check with $P_1 = 100$ and $P_2 = 1$. If P_1 is set to zero then the skyhook controller proposed by Karnopp [24, 25] is obtained.

It is to be noted that since the absolute or total displacement and velocity are needed in Equation (19), they can be obtained from measured absolute acceleration. The absolute or total displacement can be obtained using integrators/filters proposed by Spencer *et al.* [23]. The comparison of experimental and filtered absolute or total velocity and displacement under time-scaled Sylmar 90 excitation is shown in Figure 6. It is evident that the filtered absolute or total velocity and displacement is in good agreement with the recorded velocity and displacement.

RESULTS

Analytical and experimental results in the form of peak values of relative displacement responses, peak total force at the isolation level (total of friction force, MR damper force, and spring force normalized by deck weight) and deck acceleration of the sliding isolated bridge model are presented in Table II. Results under (i) El Centro, (ii) Sylmar 90, and (iii) Newhall 90 are discussed in detail. Figure 7(a) shows the peak experimental relative deck–left pier displacement response, as a function of peak table acceleration, with passive low, passive high and semi-active controlled damping cases. Figure 7(b) shows measured peak total force at the isolation level, as a function of peak table acceleration, with passive low, passive high and semi-active controlled damping cases.

As evident from Table II and Figures 7(a) and (b), in the case of Newhall 90, the deck–left pier displacement in the passive high-damping case is reduced by 27% when compared with the passive low-damping case. This occurs due to increased energy dissipation in the passive high-damping case, with a corresponding 13% increase in the total force when compared with

Table II. Peak values of analytical and experimental response of the bridge model in the high-friction case (percentage reductions in passive high-damping and controlled cases over the passive low-damping case are presented in parentheses).

		Deck–Left pier (cm)		Deck–Right pier (cm)		Left pier–Table (cm)		Right pier–Table (cm)		Total force at isolation Level/Wt.		Deck acceleration (g)	
Earthquake	MR D	Expt	Analytical	Expt	Analytical	Expt	Analytical	Expt	Analytical	Expt	Analytical	Expt	Analytical
El Centro	0 V	1.00	1.03	0.944	0.972	0.12	0.162	0.165	0.153	0.201	0.196	0.233	0.213
El Centro	4 V	0.866 (13%)	0.877 (15%)	0.922 (2%)	0.925 (5%)	0.23 (−92%)	0.271 (−67%)	0.15 (9%)	0.165 (−8%)	0.288 (−43%)	0.301 (−54%)	0.322 (−38%)	0.315 (−48%)
El Centro	Control	0.772 (23%)	0.827 (20%)	0.752 (20%)	0.878 (10%)	0.27 (−125%)	0.248 (−53%)	0.147 (11%)	0.161 (−5%)	0.272 (−35%)	0.297 (−52%)	0.32 (−37%)	0.31 (−46%)
Sylmar 90	0 V	2.208	2.034	2.191	2.045	0.172	0.143	0.174	0.136	0.42	0.42	0.264	0.317
Sylmar 90	4 V	1.77 (20%)	1.534 (25%)	1.81 (17%)	1.629 (20%)	0.268 (−56%)	0.246 (−72%)	0.168 (3%)	0.129 (5%)	0.487 (−16%)	0.464 (−10%)	0.4 (−52%)	0.381 (−20%)
Sylmar 90	Control	1.375 (38%)	1.234 (39%)	1.425 (35%)	1.322 (35%)	0.264 (−53%)	0.233 (−63%)	0.16 (8%)	0.11 (19%)	0.44 (−5%)	0.42 0%)	0.304 (−15%)	0.356 (−12%)
Newhall 90	0 V	1.516	1.905	1.53	1.919	0.193	0.144	0.146	0.133	0.372	0.41	0.34	0.24
Newhall 90	4 V	1.112 (27%)	1.03 (46%)	1.182 (23%)	1.17 (39%)	0.251 (−30%)	0.273 (−90%)	0.16 (−10%)	0.121 (9%)	0.42 (−13%)	0.44 (−7%)	0.447 (−31%)	0.356 (−48%)
Newhall 90	Control	0.841 (45%)	0.908 (52%)	0.96 (37%)	0.942 (51%)	0.21 (−9%)	0.202 (−40%)	0.19 (−30%)	0.113 (15%)	0.362 (3%)	0.362 (12%)	0.26 (24%)	0.261 (−9%)

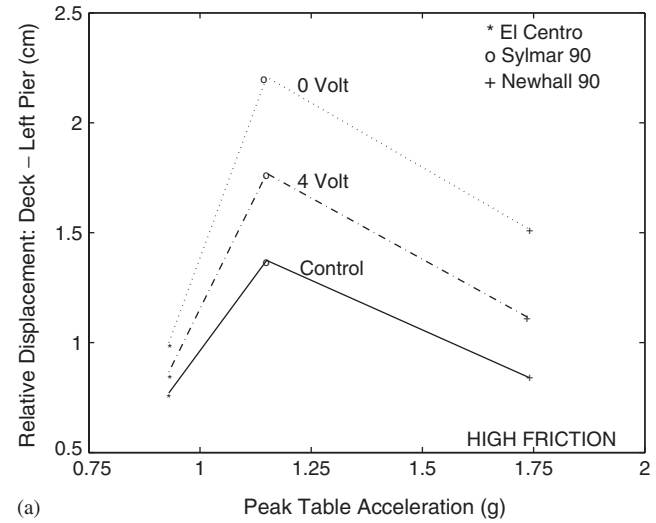

(a)

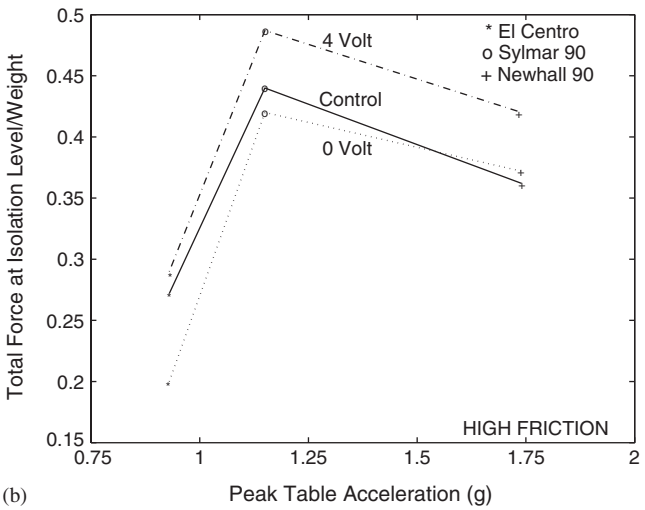

(b)

Figure 7. (a) Experimental peak relative deck–left pier displacement; and (b) measured total force at isolation level/weight as a function of peak shake table acceleration.

the passive low-damping case. It is to be noted here that the passive high-damping case reduces bearing displacements, but at the expense of increased isolation level forces and pier drifts (see Table II). The controlled case with semi-active damping, shown in Figures 7(a) and (b), reduces the deck–left pier displacement by 45% when compared to the passive low-damping case, and by 18% when compared to the passive high-damping case, while maintaining the total force at the isolation level 3% less than the passive low-damping case. Thus the control case with less energy dissipated (see Figure 8)—but more efficiently dissipated—reduces the relative deck–left pier displacement response and total force further than the passive

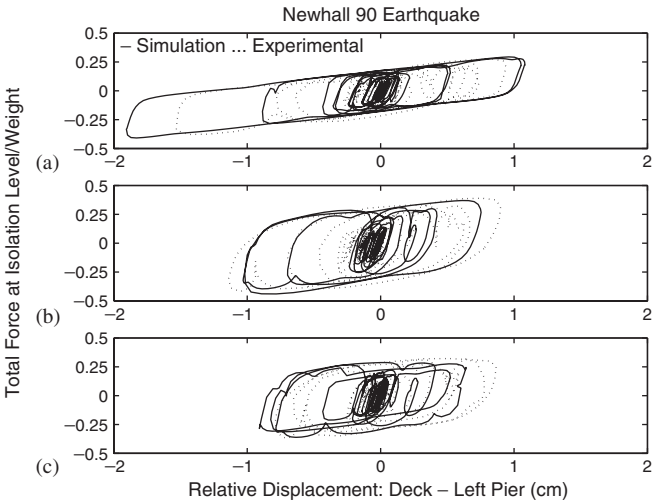

Figure 8. Total force at the isolation level—relative deck–left pier displacement plots under Newhall 90 (note: changing width of loops in the controlled case): (a) MRD 0.0 V; (b) MRD 4.0 V; and (c) MRD control.

low- and high-damping cases. Such reductions in displacements as well as isolation level forces reveal the effectiveness of smart damping. From Table II a similar set of observations can be obtained from the analytical study as well.

Table II also shows peak relative left and right pier displacements with respect to shake table and deck acceleration under the Newhall 90 earthquake with passive low, passive high and semi-active controlled damping cases. The controlled case maintains piers displacements and deck acceleration within the bounds of the passive low- and high-damping cases.

Experimental results under Sylmar 90 and El Centro earthquakes are also presented in Table II and Figures 7(a) and (b). The semi-active controlled case results in the least relative deck–left pier displacement responses when compared to the passive low- and high-damping cases, giving 38% reduction in deck–left pier displacement for Sylmar 90, and 23% reduction in deck–left pier displacement under El Centro excitation. The controlled case also reduces the total force at the isolation level by 10% under Sylmar 90 and by 6% under the El Centro earthquake, when compared to the passive high-damping case. It is also evident from Table II that the controlled case maintains the pier drifts and deck acceleration within the bounds of the two passive cases or at the same level as the passive high-damping case.

The shake table test results are presented in Figures 8 to 13 in the form of relative displacement time history responses, total force at isolation level versus relative deck–left pier displacement responses, applied voltage time history, and deck acceleration time history response for Newhall 90 and Sylmar 90 excitations. Corresponding comparisons of analytical and experimental results are also presented in Figures 8, 10, 12 and 13. Comparison of experimental relative displacement time histories under Newhall 90 excitation, presented in Figure 9, reveal substantial reductions in the controlled case. As evident from Figure 9, most of the displacement occurs at the isolation level and the pier displacements are significantly reduced. Comparison of analytical and experimental total force at the isolation level versus relative

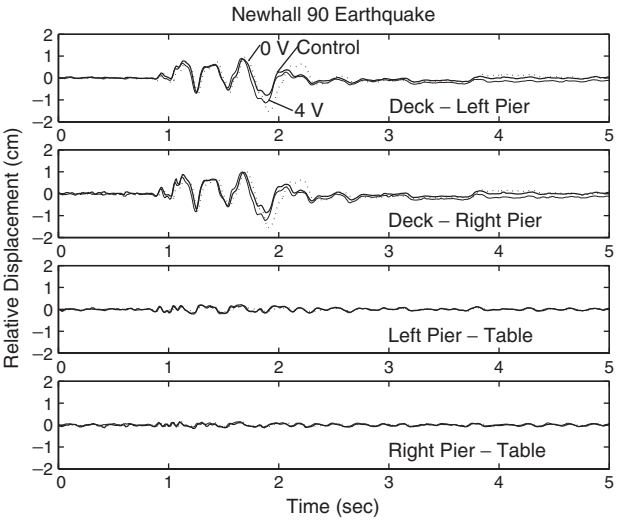

Figure 9. Comparison of experimental relative displacement responses under Newhall 90.

deck–left pier displacement responses under Newhall 90 excitation, with passive low, passive high and semi-active controlled damping cases are presented in Figure 8. From Figure 8 the following features are evident: (1) energy dissipation in the passive high-damping case is increased (Figure 8(b)), which reduces the relative deck–left pier displacement response when compared to the passive low-damping case; (2) in the controlled case with smart damping the changing width of the force–displacement loops, shown in Figure 8(c), clearly shows the adaptive nature of the MR damper, which results in efficient energy dissipation; and, (3) this adaptable nature of the MR damper reduces both the relative deck–left pier displacement and total forces when compared to the passive low- and high-damping cases. Figure 10 shows the voltage signal supplied to the MR damper and comparison of analytical and experimental deck acceleration time histories, under Newhall 90, in the semi-active controlled case. Similar observations as in Newhall 90 can be made from the Sylmar 90 response plots shown in Figures 11–13. From the peak values of responses presented in Table II and Figures 8, 10, 12 and 13, it is evident that the proposed analytical model captures the response of the sliding isolated bridge model satisfactorily.

The analytical and experimental studies under fault normal Sylmar 360 and Newhall 360 earthquakes indicated similar responses in the controlled case and the passive high-damping case [18], and hence are not shown here due to lack of space.

The bridge model was also studied under low-friction conditions [26], with sliding bearings having maximum coefficient of friction 7%, under El Centro, Sylmar 90 and Newhall 90 earthquakes. The results of this study are presented in Figures 14(a) and (b). As evident from the comparison of peak relative deck–left pier displacement as a function of peak table acceleration presented in Figure 14(a), the semi-active controlled case maintains the least relative displacement response. Figure 14(b) presents the comparison of total force at the isolation level as a function of peak table acceleration. An important observation to be made from Figure 14(b) is that the controlled case maintains the total force at the same

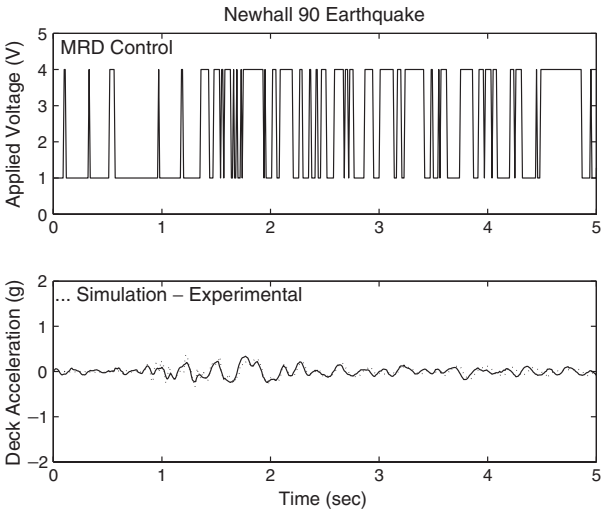

Figure 10. Voltage supplied to the MR damper in the experiment, and analytical and experimental deck acceleration response under Newhall 90.

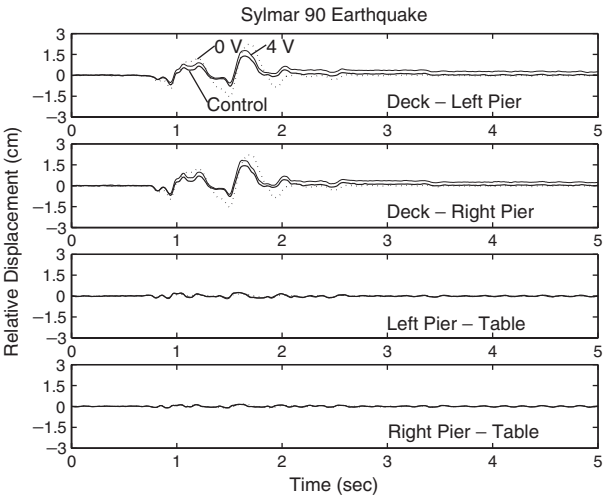

Figure 11. Comparison of experimental relative displacement response under Sylmar 90.

level as the passive low-damping case. Thus the controlled case with low-friction bearings not only reduces the bearing displacements, but also gives an added advantage by maintaining isolation level forces at the same level as the passive low-damping case. Also, the developed control algorithm is effective under high- and low-friction conditions, hence it is robust.

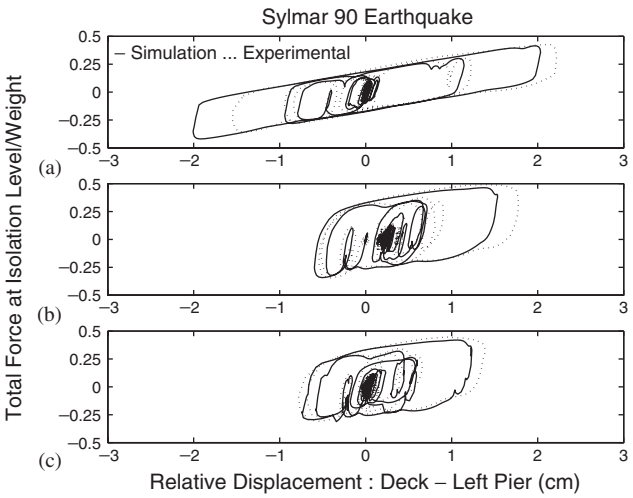

Figure 12. Total force at the isolation level—relative deck–left pier displacement plots under Sylmar 90: (a) MRD 0.0 V; (b) MRD 4.0 V; and (c) MRD control.

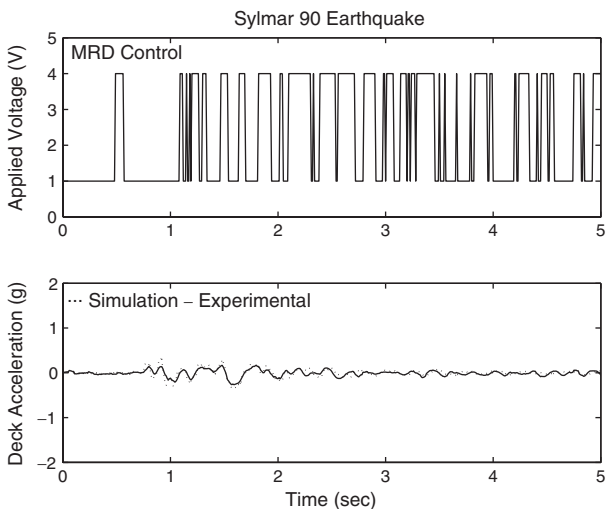

Figure 13. Voltage supplied to the MR damper in the experiment, and analytical and experimental deck acceleration response under Sylmar 90.

In summary, it can be concluded that the semi-active controlled case reduces the relative deck–left pier displacement response further than the passive low- and passive high-damping cases, while maintaining the isolation level forces lower than the passive high-damping case, in the earthquakes considered in this study.

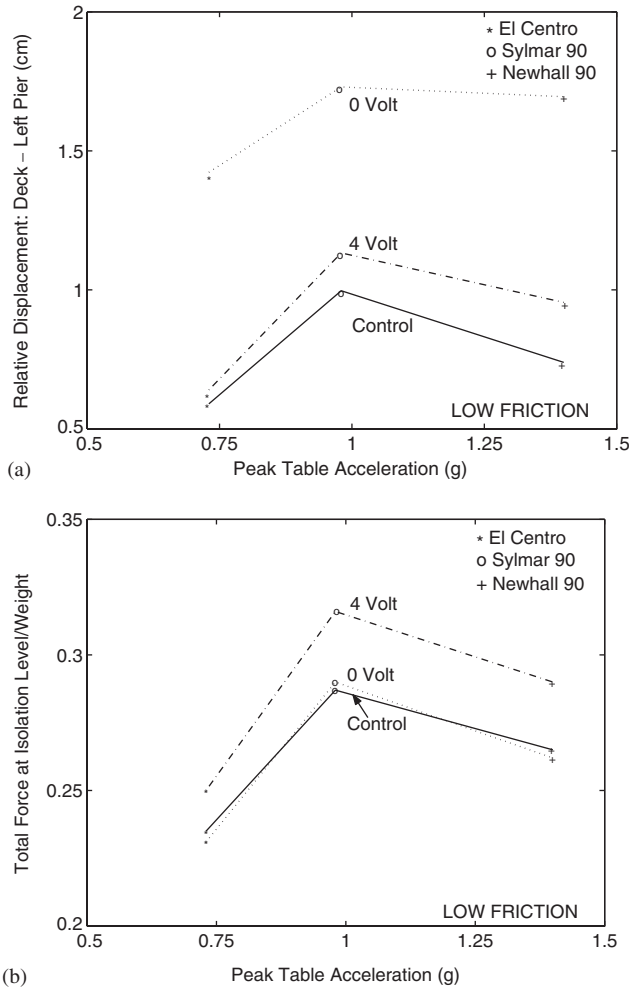

Figure 14. (a) Experimental peak relative deck–left pier displacement; and (b) comparison of peak total force/weight as a function of peak shake table acceleration.

CONCLUSIONS

A 'smart' base-isolated bridge model having sliding bearings and a MR damper is analytically and experimentally studied and shown to be effective. It is evident from the analytical and experimental study that the MR damper in the controlled mode reduces bearing displacements further than the passive low- and passive high-damping cases, while reducing isolation level forces when compared to the passive high-damping case. The main conclusions of this study are as follows: (1) In sliding isolated bridges, providing passive high-damping reduces bearing displacement, but at the expense of increased isolation level forces and pier drifts. (2) A semi-actively controlled MR damper—switching based on the developed control algorithm—reduces

bearing displacements further than passive low- and high-damping cases, while maintaining the total force at the isolation level less than the passive high-damping case. (3) Using MR dampers with low friction, the bearing displacements can be reduced further than the passive low- and high-damping cases, while maintaining isolation level forces at the same level as the passive low-damping case. Thus the controlled case with low-friction bearings has an added advantage of maintaining isolation level forces similar to the passive low-damping case. (4) The semi-active controlled case also maintains the pier drifts and deck acceleration within the bounds of the passive high- and low-damping cases. (5) The developed analytical model, with due consideration given to the non-linear characteristics of sliding bearings and the MR damper, captures the response of the bridge model satisfactorily and can be used to perform an extensive analytical study.

The developed control algorithm is effective under fault parallel components of the earthquakes considered in this study. It is demonstrated through analytical simulations and experimental tests that by providing smart dampers the performance of sliding isolated bridges can be improved.

ACKNOWLEDGEMENTS

Funding for this project, provided by the National Science Foundation, NSF-CAREER Grant CMS–9996290, is gratefully acknowledged.

REFERENCES

1. Kelly JM. *Earthquake-resistant Design with Rubber*. 2nd Edn, Springer: New York, 1997.
2. Chopra AK. *Dynamics of Structures*: *Theory and Applications to Earthquake Engineering*. 2nd Edn, Prentice Hall: New York, 2002.
3. Makris N. Rigidity–plasticity–viscosity: Can electrorheological dampers protect base-isolated structures from near-source ground motions? *Earthquake Engineering and Structural Dynamics* 1997; **26**:571–591.
4. Shen J, Tsai M, Chang K, Lee G. Performance of a seismically isolated bridge under near-fault earthquake ground motions. *Journal of Structural Engineering* (ASCE) 2004; **130**(6):861–868.
5. Tsopelas P, Okamoto S, Constantinou MC, Ozaki D, Fujii S. *Experimental and Analytical Study of Systems Consisting of Sliding Bearings*, *Rubber Restoring Devices and Fluid Dampers. Volume I. Report No. NCEER-94-0002*, National Center for Earthquake Engineering Research, State University of New York, Buffalo, NY, 1994.
6. Makris N, Zhang J. Seismic response analysis of a highway overcrossing equipped with elastomeric bearings and fluid dampers. *Journal of Structural Engineering* (ASCE) 2004; **130**(6):830–845.
7. Spencer BF, Nagarajaiah S. State of the art structural control. *Journal of Structural Engineering* (ASCE) 2003; **129**(7):845–856.
8. Kawashima K, Unjoh S. Seismic response control of bridges by variable dampers. *Journal of Structural Engineering* (ASCE) 1994; **9**:2583–2601.
9. Yang JN, Wu JC, Kawashima K, Unjoh S. Hybrid control of seismic-excited bridge structures. *Earthquake Engineering and Structural Dynamics* 1995; **24**:1437–1451.
10. Symans MD, Kelly SW. Fuzzy logic control of bridge structures using intelligent semi-active seismic isolation systems. *Earthquake Engineering and Structural Dynamics* 1999; **28**:37–60.
11. Carlson JD, Chrzan MJ. Magnetorheological Fluid Dampers. *U.S. Patent #5 277 281*; 1994.
12. Spencer BF, Dyke SJ, Sain MK, Carlson JD. Phenomenological model of a magnetorheological damper. *Journal of Engineering Mechanics* (ASCE) 1997; **123**(3):230–238.
13. Jung H, Spencer BF, Lee I. Control of seismically excited cable-stayed bridge employing magnetorheological fluid dampers. *Journal of Structural Engineering* (ASCE) 2003; **129**(7):873–883.
14. Jung HJ, Park KS, Spencer BF, Lee IW. Hybrid seismic protection of cable-stayed bridges. *Earthquake Engineering and Structural Dynamics* 2004; **33**:795–820. DOI: 10.1002/eqe.374.
15. Agrawal AK, Yang JN, He WL. Applications of some semiactive control systems to benchmark cable-stayed bridge. *Journal of Structural Engineering* (ASCE) 2003; **129**(7):884–894.

16. Gavin HP. Control of seismically excited vibration using electrorheological materials and Lyapunov methods. *IEEE Transactions on Automatic Control* 2001; **9**(1):27–36.
17. Nagarajaiah S, Riley MA, Reinhorn AM. Control of sliding isolated bridge with absolute acceleration feedback. *Journal of Engineering Mechanics* (ASCE) 1993; **119**(11):2317–2332.
18. Sahasrabudhe S. *Semi-active Control of Sliding Isolated Buildings and Bridges with Variable Stiffness and Damping Systems*. Ph.D. Thesis, Rice University, Houston, Texas, U.S.A., 2002.
19. Mills RS, Krawinkler H, Gere JM. *Model Tests on Earthquake Simulators Development and Implementation of Experimental Procedures*. Report No. 39, John A. Blume Earthquake Engineering Center, Stanford University, 1979.
20. Wen YK. Method of random vibration of hysteretic systems. *Journal of Engineering Mechanics* (ASCE) 1976; **102**(2):249–263.
21. Nagarajaiah S, Reinhorn AM, Constantinou MC. *3D-BASIS*: *Nonlinear Dynamic Analysis of Three-dimensional Base Isolated Structures—Part II*; *Report No. NCEER-91-0005*, National Center for Earthquake Engineering Research, SUNY, Buffalo, New York, 1991.
22. Nagarajaiah S, Reinhorn AM, Constantinou MC. Nonlinear dynamic analysis of 3D-base isolated structures. *Journal of Structural Engineering* (ASCE) 1991; **117**(7):2035–2054.
23. Spencer BF, Dyke SJ, Deoskar HS. Benchmark problems in structural control: Part I—Active mass driver system. *Earthquake Engineering and Structural Dynamics* 1998; **27**:1127–1139.
24. Karnopp D. Active damping in road vehicle suspension systems. *Vehicle System Dynamics* 1983; **12**(6): 291–311.
25. Karnopp D. Active and semiactive vibration isolation. *Journal of Mechanical Design* (ASME) 1995; **117**: 177–185.
26. Nagarajaiah S, Sahasrabudhe S, Iyer R. Seismic response of sliding isolated bridges with MR dampers. *Proceedings of the American Control Conference* 2000; Chicago, CD-ROM.

